Materials Research Bulletin 48 (2013) 3474–3478

Contents lists available at SciVerse ScienceDirect

Materials Research Bulletin

journal homepage: www.elsevier.com/locate/matresbu

One-step room temperature synthesis of very small γ-Fe_2O_3 nanoparticles

O. Moscoso-Londoño [a], M.S. Carrião [a,b], C. Cosio-Castañeda [a,c], V. Bilovol [a], R. Martínez Sánchez [d], E.J. Lede [a], L.M. Socolovsky [a], R. Martínez-García [a,*]

[a] Laboratorio de Sólidos Amorfos, INTECIN, Facultad de Ingeniería, Universidad de Buenos Aires, C1063ACV, Buenos Aires, Argentina
[b] Instituto de Física, Campus II, Universidade Federal de Goiás, CEP: 74001-970 Goiânia (GO), Brazil
[c] Departamento de Física y Química Teórica, Facultad de Química, Universidad Nacional Autónoma de México, Ciudad Universitaria, D.F. 04510, Mexico
[d] Instituto de Materiales y Reactivos, Universidad de La Habana, CP10400, Ciudad Habana, Cuba

ARTICLE INFO

Article history:
Received 3 December 2012
Received in revised form 7 May 2013
Accepted 10 May 2013
Available online 18 May 2013

Keywords:
A. Oxides
B. Chemical synthesis
C. Mössbauer spectroscopy
C. XAFS (EXAFS and XANES)

ABSTRACT

Very small maghemite nanoparticles (~3 nm) are obtained through a one-step synthesis at room temperature. The fast neutralization reaction of a ferric solution in a basic medium produces an intermediate phase, presumably two-line ferrihydrite, which in oxidizing conditions is transformed to maghemite nanoparticles. The synthesis of maghemite, as final product of the reaction, was characterized by High-Resolution Transmission Electron Microscopy (HR-TEM), X-ray Absorption Fine Structure (XAFS), Mössbauer spectroscopy, and magnetometry. The XAFS technique allowed the analysis of the crystallographic variations into maghemite nanoparticles as a result of modification in its surface/volume ratio. Mössbauer spectroscopy at low temperature (4.2 K) confirms the presence of Fe(III) in tetrahedral and octahedral interstices, in the stoichiometry corresponding to maghemite. The specific magnetization, M vs H (3 K and 300 K, up to 7 T) and temperature dependence of the magnetization (50 Oe by ZFC mode, $2\ K \leq T \leq 300\ K$) indicate that maghemite nanoparticles of 3 nm are in superparamagnetic state with a blocking temperature close to 36 K

© 2013 Elsevier Ltd. All rights reserved.

1. Introduction

Iron oxide nanoparticles (NPs) have been the subject of many studies due to their great importance in several technological applications, which range from information data storage to biological and biomedical applications [1–3]. Of these oxides, maghemite (γ-Fe_2O_3) is one of the most used because its magnetic properties and chemical stability. In bulk, γ-Fe_2O_3 is ferrimagnetic at room temperature since its inverse spinel crystal structure has two sublattices where Fe(III) ions are in different oxygen environments. However, when γ-Fe_2O_3 NPs are smaller than 5 nm, the magnetic behavior at room temperature is superparamagnetic.

Diverse routes for synthesizing γ-Fe_2O_3 NPs are reported: sol-gel synthesis [4], electron beam deposition [5], mechanochemical synthesis [6] and pyrolysis [7], among others. However, the conventional method to obtain γ-Fe_2O_3 NPs is the oxidation of magnetite [8,9] in where particles size exceeds 12 nm. In this way, it is desirable a direct method to synthesize smaller NPs.

Ferric salt hydrolysis generates an oxyhydroxide, akaganeite or two-line ferrihydrite, that depends strongly on the thermodynamics conditions (pH, temperature, concentration, stirring velocity, etc.) [10–13]. Obtaining of two-line ferrihydrite is favored if synthesis, in basic medium, is done at room temperature and ferric solution aging is avoid [11,12,14–25].

This is relevant because the α-Fe_2O_3 or γ-Fe_2O_3 formation in aqueous medium depends on the oxyhydroxide precursor. If akaganeite is the precursor, α-Fe_2O_3 is obtained, but if two-line ferrihydrite is the precursor, is possible to stabilize γ-Fe_2O_3 [26–28]. The possibility to obtain γ-Fe_2O_3 from two-line ferrihydrite is based on structural similarity that may exist between these two phases. Nevertheless, there is a controversy about the existence of tetrahedral Fe (III) in two-line ferrihydrite [11,29–33]. One of the aims of this work is to provide new facts to such discussion.

This paper gives evidences about the transformation of two-line ferrihydrite in maghemite, as well as support the hypothesis of the existence of Fe(III) tetrahedral in two-line ferrihydrite. Furthermore, a one-step synthesis of 3 nm maghemite nanoparticles, based on hydrolysis of iron (III) chloride at room temperature is reported.

2. Materials and methods

Ferric chloride solution (0.8 M) was slowly dropped in 40 ml of 28% ammonia solution until pH = 9 is reached. The aqueous

* Corresponding author at: Paseo Colón 850, Ciudad Autónoma de Buenos Aires, C1063ACV, Buenos Aires, Argentina. Tel.: +54 911 4343 0893; fax: +54 911 4343 0092x232.
E-mail address: rmartinez@fi.uba.ar (R. Martínez-García).

0025-5408/$ – see front matter © 2013 Elsevier Ltd. All rights reserved.
http://dx.doi.org/10.1016/j.materresbull.2013.05.042

solution was stirred at 500 rpm by 2 h. The solid precipitated was filtered and washed with distilled water in order to remove ammonium chloride. Finally, the product was spread onto a glass to improve drying and oxidation at room temperature. The final solid (we will name it "experimental sample") was characterized by High Resolution Transmission Electron Microscopy (HR-TEM), X-ray Absorption Fine Structure (XAFS), Mössbauer spectroscopy and Magnetometry. A reference sample, composed of 10 nm maghemite nanoparticles, was synthesized following the method reported by Jawad and Ashraf [34]. In order to confirm the composition of the reference sample, X-ray powder diffraction analysis was done.

The HR-TEM images were obtained using a JEOL 3010 microscope with a resolution of 1.7 Å. The beam used to do XAFS measurements was collimated with a slit of 0.2 mm, and monochromatized with a double crystal of Si (111). This configuration provides a resolution of 1.2 eV. The energy of monochromator was calibrated with the K-edge position of Fe foil at 7.112 keV. Spectra were normalized in the pre-edge region with a linear function, and in the post-edge region with a polynomial of degree two. XAFS data were collected in the transmission mode at 10 K, in order to avoid noise by thermal factors. To prepare sample for XAFS measurement, appropriated amounts of sample and boron nitride were mixed to reach a dilution in order to obtain an edge jump ($\Delta\mu/\mu$) close to 1.

A Mössbauer spectrum was measured at 4.2 K in a constant acceleration spectrometer operated in transmission mode with a ^{57}Co:Rh source. The obtained data were fitted using a least-square minimization algorithm and a Lorentzian line shape in order to obtain the hyperfine parameters. Isomer shifts were referred to the centroid of the spectrum of α-Fe at room temperature.

Magnetic characterization was done by using a SQUID magnetometer. The magnetization versus applied magnetic field was done at 5 K and 300 K, up to 7 T. Temperature dependence of magnetization was measured between 5 and 300 K in zero field cooling and field cooling modes.

3. Results and discussion

The analysis of HR-TEM images shows that the experimental sample is composed by very tiny particles with small size distribution. A histogram was built analyzing NPs size in TEM images (Fig. 1), and as result, a mean diameter of 3.3 ± 0.7 nm was obtained. By the Fast Fourier Transformation (FFT) technique a common feature is observed in most of the FFT graphs corresponding to the nanoparticles with diameters less than 3 nm. Usual measured interplanar distances, d = 2.5 Å (plane (3 1 1)) and 2.2 Å (plane (3 2 1)), are in good agreement with distances of maghemite crystal [35]. However, most of the measured angles between those planes have different values if compared with those calculated from the established relationships with plane indexes [36]. Such effect is associated with disorder due to surface/volume ratio, in where the atoms located in the surface are not in the regular configuration as is in a bulk crystal. For example, in a 2 nm NP the number of unit cells on the surface represents approximately 88% of total volume (Fig. 1b, inset).

The normalized XANES spectra corresponding to experimental sample (black line) and 10 nm γ-Fe_2O_3 NPs, as reference (gray line), are shown in Fig. 2. The similitude of both profiles suggests that experimental sample is composed by maghemite. The XANES spectra are in good agreement with those observed by Wilke et al. [36]. However, there are some difference associates with the particle size. When surface/volume ratio increases, the spectrum becomes smeared due to the increase in the surface distribution of sites.

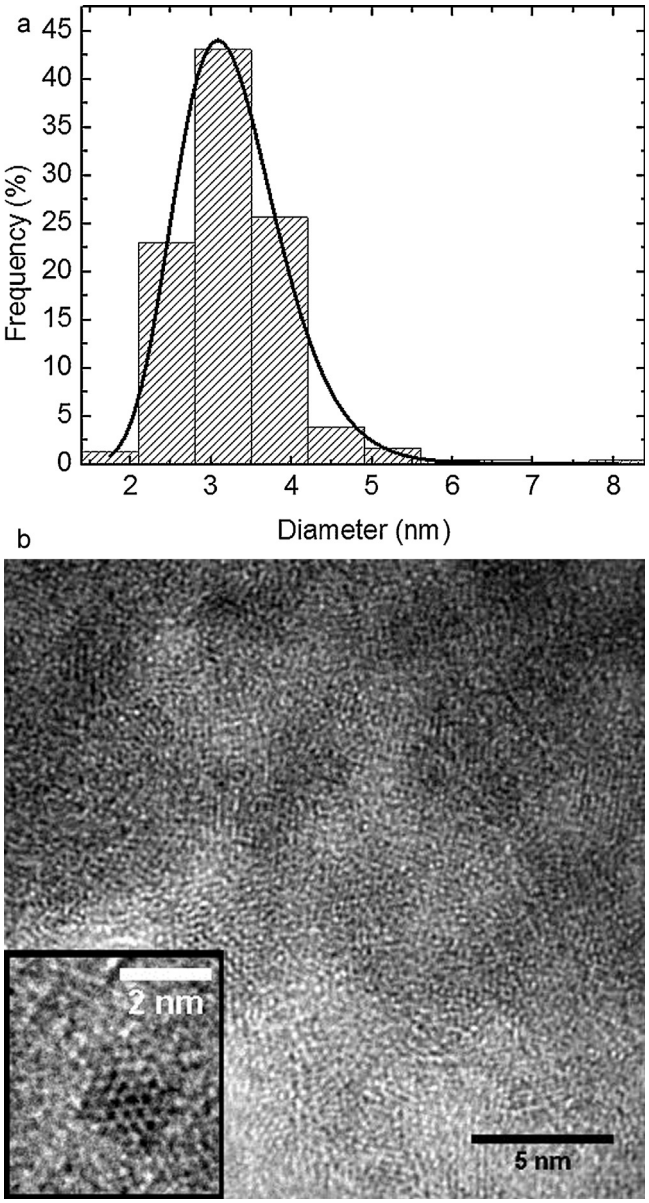

Fig. 1. (a) Histogram (bars) and lognormal fit (line) of nanoparticle size distribution. (b) HR-TEM image of maghemite nanoparticles. Inset: detail of a 2 nm NP.

The EXAFS region and Fourier transform for the experimental sample and reference system are showed in Fig. 3. EXAFS profiles exhibit a characteristic signal (obtained by conventional treatment) formed by the contribution of the first and second oxygen neighbor as well as Fe (III) ions. The Fourier transform shows an intense peak characteristic, generated by first and second O–Fe neighbors (0.83–2.1 Å) and less intense peaks associated with more distant neighbors (2.1–3.5 Å). This last signal corresponding to the second coordination sphere and its intensity increase as the particle size grows. This would be indicating an increase in average coordination number and a higher order in the medium range (as expected due to the reduction of size). In brief, the comparison of the XANES spectra between experimental sample with the reference system (γ-Fe_2O_3-10 nm) and with the literature reports [37], leads us to conclude that experimental sample is compatible with γ-Fe_2O_3. It is also important to note that when increasing the surface/volume ratio, the number of iron atoms in the surface is greater and coordination decreases on average.

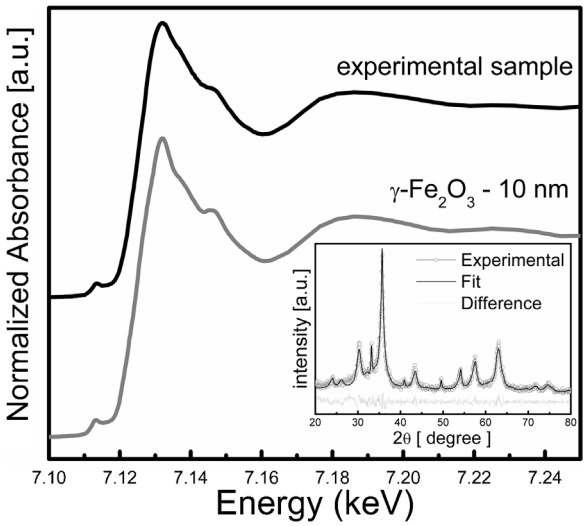

Fig. 2. XANES spectra for experimental sample (black line) and reference system γ-Fe_2O_3 (gray line). Inset: Experimental X-ray diffraction pattern and the corresponding fit (CIF file number: 9006317 [38]) for the reference system γ-Fe_2O_3.

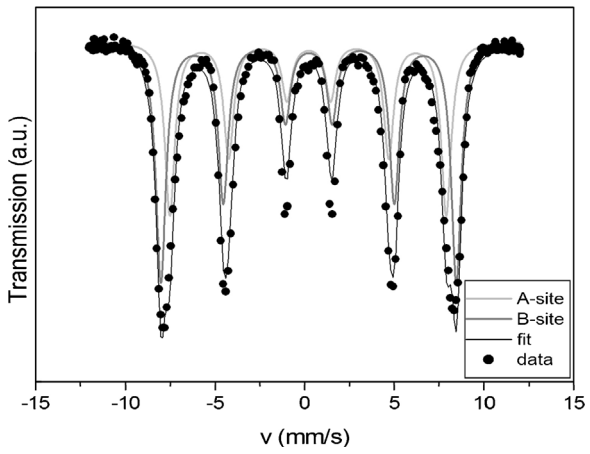

Fig. 4. 4.2 K Mössbauer spectrum of the sample with its corresponding fitting curves (tetrahedral A-site and octahedral B-site).

The study of the structure and transformation of two-line ferrihydrite has more than two decades of discussion for the controversial existence of tetrahedral Fe (III) in two-line ferrihydrite. First, Drits et al. [39], Manceau et al. [40], Jansen et al. [41] and Hiemstra [42], refer that iron atoms are only in octahedral interstices. Whilst, Eggleton et al. [32], Michel et al. [43,44], Maillot et al. [45] and Peak et al. [29] report that a significant fraction of Fe(III) are in tetrahedral sites.

In this way, Mössbauer spectrum of the experimental sample (Fig. 4) was measured in order to get information about the environments of Fe(III). The 4.2 K Mössbauer spectrum allows identification of iron oxide because, at this low temperature, the nanoparticle magnetic supermoments are blocked and the spectrum is magnetically split [46]. The analysis of the spectrum shows that the sample consists of crystalline maghemite. For the fitting procedure, two Lorentzian-shaped sextets (48.1 T and 51.4 T) were used [47]. Obtained isomer shifts δ are 0.39 mm/s and 0.46 mm/s, which correspond to Fe(III) in tetrahedral and octahedral environment, respectively, of maghemite at this temperature and are in a good agreement with those reported previously [48–50]. The line width Γ = 0.67 mm/s corroborates the fact that we deal with extremely small γ-Fe_2O_3 NPs and it is justified by the diversity of the iron probe environments due to a high surface/volume ratio. As it can be appreciated from Fig. 1a, nearly 40% of nanoparticles have their size below 3 nm.

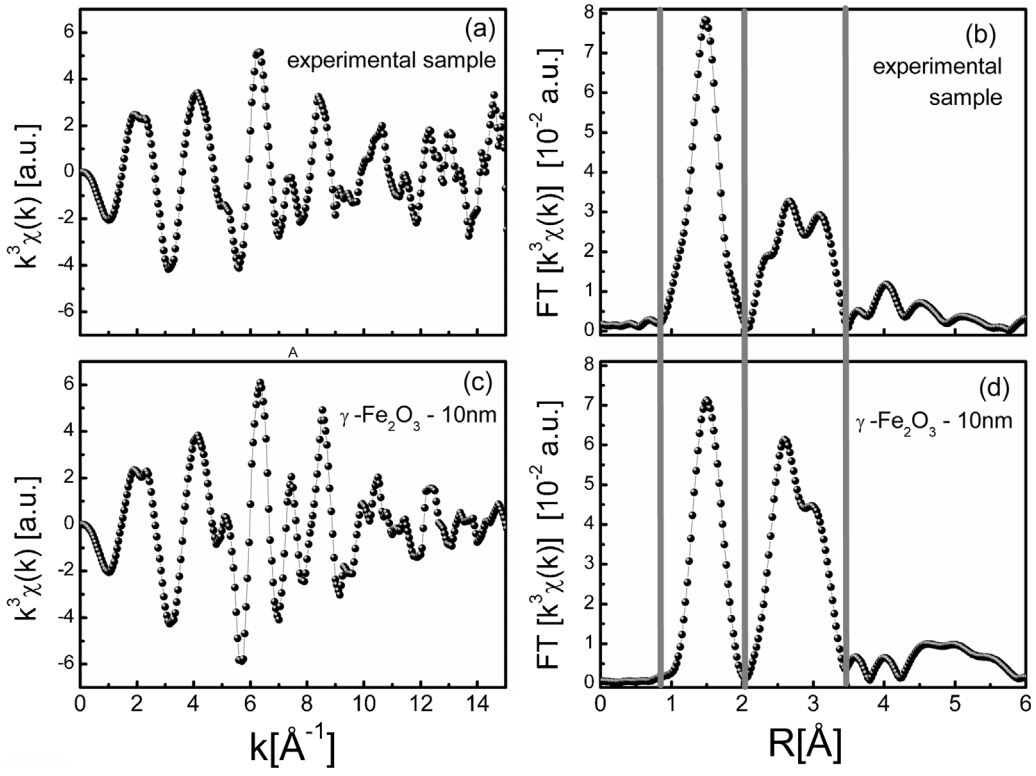

Fig. 3. EXAFS spectra and Fourier transforms obtained for the experimental sample (a and b) and reference system (c and d).

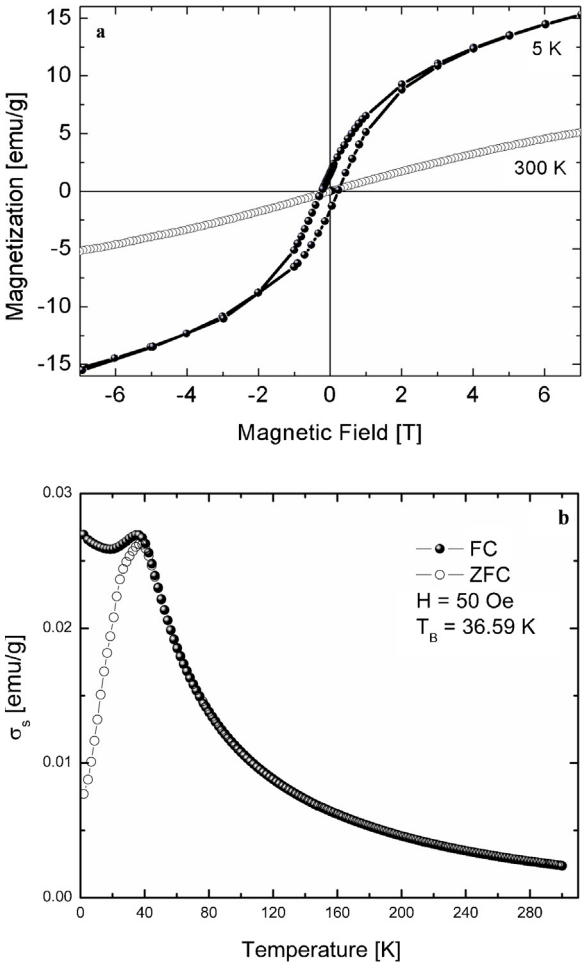

Fig. 5. (a) M. vs H behavior by the experimental sample at 300 K (empty circles) and 5 K (full circle). Their shapes are characteristic of a superparamagnetic system. (b) ZFC and FC curves by experimental sample. Superparamagnetism features are clearly seen. Blocking temperature, T_B, is at 36 K. The irreversible temperature is almost the same as T_B. This is indicative of a small nanoparticles size distribution.

Magnetizations vs. applied magnetic field (M vs. H) measurements were performed at 300 K and 5 K (Fig. 5a). As can be seen, magnetization does not saturate even at 7 T. Both curves are S-shaped. Those features are characteristic of superparamagnetic systems [46]. The low temperature curve shows hysteretic behavior with specific magnetization (σ_S) at 7 T close to 15 emu/g. Similar values of magnetization have been reported by Glaria et al. for 3 nm [51], and by Mercante for 4 nm γ-Fe_2O_3 NPs [50]. The reduction of magnetization in comparison to the bulk saturation value (about 76 emu/g [52]) is attributed to magnetic moments canting and a large disordered spin surface, as expected for particles of a few nanometers due to the high surface to core ratio, which promote broken bonds and frustrations of antiferromagnetic superexchange interactions [53,54]. In M vs. H curve at T = 300 K the specific magnetization at 7 T is even smaller (around 5 emu/g), as corresponds to an unblocked state. Specific magnetization measured at 5 and 300 K is higher than those reported for hematite and most of the iron oxides, except magnetite and maghemite, [55–57]. This confirms that experimental sample is composed by maghemite (there not magnetite because there not Fe(II) involved in synthesis). M vs. H curve at 5 K shows a considerable increase in the coercive field, which indicates that the system is in superparamagnetic blocked regime [46].

Zero-field-cooled (ZFC) and field-cooled (FC) DC magnetization curves are showed in Fig. 5b. A blocking temperature (T_B) of 36 K was obtained. The uniaxial anisotropy constant for an ideal superparamagnetic system (K) was estimated through the equation $T_B = KV/25k_B$, where V is the volume of nanoparticle, and k_B is the Boltzmann constant [46]. The calculated value of K was 8.25×10^5 erg/cm^3, which is in good agreement with values reported for γ-Fe_2O_3 NPs of similar sizes [9]. The FC curve shape at low temperatures (below T_B), indicates that we are dealing with an interacting system, which is expected in a system that is composed by NPs that are in close contact. In that way, other magnetic interactions, different from the dipolar one, are presents. For instance, direct interchange interaction between atoms in different nanoparticles in contact. This has influence on the blocking temperature of the system, shifting it to higher temperatures [46].

4. Conclusion

Very small maghemite nanoparticles (~3 nm) can be synthesized by co-precipitation in a one-step reaction (neutralization process of a ferric solution). The maghemite, as a final product, can be obtained only if the precursor has Fe(III) in tetrahedral interstices. HR-TEM, XAFS, and Mössbauer spectroscopy confirm that experimental sample is composed of nanoparticles that have the crystalline structure of maghemite, compatible with its small sizes. The corresponding electronic change of the coordination sphere of Fe(III) due to the surface/volume ratio of the nanoparticles was observed by the XANES and EXAFS spectra. As expected these nanoparticles are superparamagnetic with a small blocking temperature.

Acknowledgements

Agencies of Argentine (CONICET and ANPCyT (PICT 280-08 and CU1006)), Colombia (COLCIENCIAS), and Mexico (CONACyT), are acknowledged for financial support. National Synchrotron Light Laboratory (LNLS, CNPEM, Campinas, Brazil) is acknowledged for the use of the XAS beamline and HR-TEM (Electron Microscopy Laboratory, C2NANO, CNPEM, Campinas, Brazil). Also we thank R. Cohen and L. Nagamine (LMM, USP, Brazil) for Mössbauer measurements.

References

[1] G. Reiss, A. Hütten, Nat. Mater. 4 (2005) 725–726.
[2] Q.A. Pankhurst, J. Connolly, S.K. Jones, J. Dobson, J. Phys. D: Appl. Phys. 36 (2003) R167–R181.
[3] V.I. Shubayev, T.R. Pisanic, S. Jin, Adv. Drug Deliv. Rev. 61 (2009) 467–477.
[4] D. Ortega, R. García, R. Marín, C. Barrera-Solano, E. Blanco, M. Domínguez, M. Ramírez-del-Solar, Nanotechnology 19 (2008) 475706.
[5] S. Jain, A.O. Adeyeye, S.Y. Chan, C.B. Boothroyd, J. Phys. D: Appl. Phys. 37 (2004) 2720–2725.
[6] T. Tsuzuki, F. Schäffel, M. Muroi, P.G. McCormick, J. Alloys Compd. 509 (2011) 5420–5425.
[7] C.R. Lin, R.K. Chiang, J.S. Wang, T.W. Sung, J. Appl. Phys. 99 (2006) 08N710.
[8] F. Schüth, M. Hesse, K.K. Unger, Precipitation and coprecipitation, in: Handbook of Heterogeneous Catalysis, Wiley-VCH Verlag GmbH & Co. KGaA, Germany, 2008.
[9] J. Jong-Ryul, S. Sung-Chul, L. Seung-Jun, K. Jong-Duk, J. Magn. Magn. Mater. 286 (2005) 5–9.
[10] C.M. Flynn Jr., Chem. Rev. 84 (1984) 31–41.
[11] A. Manceau, Am. Miner. 96 (2011) 521–533.
[12] A. Šarić, S. Musić, K. Nomura, S. Popvić, Croat. Chem. Acta 71 (1998) 1019–1038.
[13] M. Mohapatra, S. Anand, Int. J. Eng. Sci. Technol. 2 (2010) 127–146.
[14] J.L. Jambor, J.E. Dutrizac, Chem. Rev. 98 (1998) 2549–2585.
[15] U. Schwertmann, R.M. Cornell, Iron Oxides in the Laboratory, VCH publishers, New York, 1991.
[16] H. Maeda, Langmuir 12 (1996) 1446–1452.
[17] T.D. Glotch, M.D. Kraft, Phys. Chem. Miner. 35 (2008) 569–581.
[18] J.A. Jaén, J. Iglesias, C. Hernández, Int. J. Corrosion ID 162729 (2012) 1–11.
[19] J.J. Santana Rodríguez, F.J. Santana Hernández, J.E. González, Corrosion Sci. 44 (2002) 2425–2438.
[20] B. Weckler, H.D. Lutz, Eur J. Solid State Inorg. Chem. 35 (1998) 531–544.
[21] R. Parameshwari, P. Priyadarshini, G. Chandrasekaran, Am. J. Mat. Sci. 1 (2011) 18–25.

[22] L.M. Meng, K. Hyung-Hwan, K. Hyuck, M. Mamoun, K.D. Kyung, Nano. Rev. 1 (2010) 4883.
[23] K. Rout, M. Mohapatra, S. Anand, Dalton Trans. 41 (2012) 3302–3312.
[24] U. Schwertmann, E. Murad, Clays Clay Miner. 31 (1983) 277–284.
[25] J. Zhao, F.E. Huggins, Z. Feng, G.P. Huffman, Clays Clay Miner. 42 (1994) 737–746.
[26] A.N. Christensen, T.R. Jensen, C.R.H. Bahl, E. DiMasi, J. Solid State Chem. 180 (2007) 1431–1435.
[27] F. Meng, S.A. Morin, S. Jin, J. Am. Chem. Soc. 133 (2011) 8408–8411.
[28] C. Carbone, F. Di Benedetto, P. Marescotti, C. Sangregorio, L. Sorace, N. Lima, M. Romanelli, G. Lucchetti, C. Cipriani, Miner. Petrol. 85 (2005) 19–32.
[29] D. Peak, T. Regier, Environ. Sci. Technol. 46 (2012) 3163–3168.
[30] V. Barrón, J. Torrent, Geochim. Cosmochim. Acta 66 (2002) 2801–2806.
[31] Q. Liu, V. Barrón, J. Torrent, S.G. Eeckhout, C. Deng, J. Geophys. Res. 113 (2008) B01103.
[32] R.A. Eggleton, R.W. Fitzpatrick, Clays Clay Miner. 36 (1998) 111–124.
[33] H. Tüysüz, E.L. Salabaş, C. Weidenthaler, F. Schüth, J. Am. Chem. Soc. 130 (2008) 280–287.
[34] A. Jawad, S.S.Z. Ashraf, Eur. Phys. J. Appl. Phys. 54 (2011) 10402.
[35] H.-S. Shin, Y. Hakhoechi, Powder Diffraction 35 (1998) 1113, File #89-5892. ICDD.
[36] M. Wilke, F. Farges, P.E. Petit, G. Brown Jr., F. Martin, Am. Miner. 86 (2001) 714–730.
[37] J.W. Edington, Electron Diffraction in the Electron Microscope, Practical Electron Microscopy in Materials Science, Philips Technical Library, Macmillan Press Ltd., London, 1975.
[38] C. Pecharromán, T. González-Carreño, J.E. Iglesias, Phys. Chem. Miner. 22 (1995) 21–29, CIF 0631907.
[39] V.A. Drits, B.A. Sakharov, A.L. Salyn, A. Manceau, Clay Miner. 28 (1993) 185–207.
[40] A. Manceau, V.A. Drits, Clay Miner. 28 (1993) 165–184.
[41] E. Jansen, A. Kyek, W. Schäfer, U. Schwertmann, Appl. Phys. A 74 (2002) S1004–S1006.
[42] T. Hiemstra, W.H. van Riemsdijk, Geochim. Cosmochim. Acta 73 (2009) 4423–4436.
[43] F.M. Michel, L. Ehm, S.M. Antao, P.L. Lee, P.J. Chupas, G. Liu, D.R. Strongin, M.A.A. Schoonen, B.L. Phillips, J.B. Parise, Science 316 (2007) 1726–1729.
[44] F.M. Michel, V. Barrón, J. Torrent, M.P. Morales, C.J. Serna, J.F. Boily, Q. Liu, A. Ambrosini, A.C. Cismasu, G.E. Brown Jr., Proc. Natl. Acad. Sci. U.S.A. 170 (2010) 2787–2792.
[45] F. Maillot, G. Morin, Y. Wang, D. Bonnin, P. Ildefonse, C. Chaneac, G. Calas, Geochim. Cosmochim. Acta 75 (2011) 2708–2720.
[46] M. Knobel, W.C. Nunes, L.M. Socolovsky, E. De Biasi, J.M. Vargas, J.C. Denardin, J. Nanosci. Nanotechnol. 8 (2008) 2836–2857.
[47] F. Bodker, M.F. Hansen, C.B. Koch, K. Lefmann, S. Mørup, Phys. Rev. B 61 (2000) 6826–6838.
[48] L.I. Casas, A. Roig, E. Molins, J.-M. Grenèche, J. Asenjo, J. Tejeda, Appl. Phys. A 74 (2002) 591–597.
[49] P.M.A. de Bakker, E. De Grave, R.E. Vandenberghe, L.H. Bowen, R.J. Pollard, R.M. Persoons, Phys. Chem. Miner. 18 (1991) 131–143.
[50] L.A. Mercante, W.W.M. Melo, M. Granada, H.E. Troiani, W.A.A. Macedo, J.D. Ardison, M.G.F. Vaz, M.A. Novak, J. Magn. Magn. Mater. 324 (2012) 3029–3033.
[51] A. Glaria, M.L. Kahn, A. Falqui, P. Lecante, V. Collière, M. Respaud, B. Chaudret, Chem. Phys. Chem. 9 (2008) 2035–2041.
[52] C.O. Handley, Modern Magnetic Material: Principles and Applications, Wiley-Interscience, New York, 2000.
[53] D. Bonacchi, A. Caneschi, D. Dorignac, A. Falqui, D. Gatteschi, D. Rovai, C. Sangregorio, R. Sessoli, Chem. Mater. 16 (2004) 2016–2020.
[54] M.P. Morales, S. Veintemillas-Verdaguer, M.I. Montero, C.J. Serna, A. Roig, L. Casas, B. Martínez, F. Sandiumenge, Chem. Mater. 11 (1999) 3058–3064.
[55] T.S. Berquó, S.K. Banerjee, R.G. Ford, R.L. Penn, T. Pichler, J. Geophys. Res. 112 (2007) B02102.
[56] Y. Guyodo, S.K. Banerjee, R.L. Penn, D. Burleson, T.S. Berquo, T. Seda, P. Solheid, Phys. Earth Planet. Inter. 154 (2006) 222–233.
[57] G.H. Lee, S.H. Kim, B.J. Choi, S.H. Huh, J. Korean Phys. Soc. 45 (2004) 1019–1024.